Wind field retrieval from L-band SAR mimicking future ROSE-L acquisitions

RL2OCEAN

G. Grieco [1], M. Portabella [2], F. Cossu [2], E. Makarova [2]. R. Suñe-Gonzalez [2], A. Mouche [3], A. Grouazel [3], Q. Febvre [3], M. W. Hansen [4], A. Rabaneda [4], F. Nunziata [5], D. Comite [5], A. Valentino [6], M. Pinheiro [6], L. Iannini [6], Y. Zhu [7]

19th May 2026

[1]CNR-ISMAR, [2]CSIC-ICM, [3]IFREMER, [4]MetNo, [5]SUR, [6]ESA-ESRIN, [7]Tsinghua University,

Outline

- ROSE-L overview
- **ROSE-L Level 2 Ocean (RL2Ocean)** objectives
- **ROSE-L Ocean Science Study (Rachel-ROSS)** objectives
- Wind retrieval scheme
- Development plan

ROSE-L overview

- **ROSE-L: Radar Observing System for Europe** in L-band
- L-band SAR with **Multiple Azimuth Phase Centers (MAPS)**
- Mission aims: synergy with S-1 over land, ocean and ice
- Four acquisition modes:
  - **Wave Mode (WV)**: 20x20 km^2 stripmap(or scansar?) vignettes Single Pol
  - **ROSE-L Interferometric Wide Swath (RIWS)**: 260 km-wide Dual Pol
  - **ROSE-L Extended Wide Swath (REWS)**: 400 km-wide Dual Pol
  - **ROSE-L Quad-Pol Wide Swath (QWS)**: 260 km-wide Quad Pol

RL2Ocean objectives:

- Definition of **L2 OCN** products and their algorithms
- Consolidation of **Cal/Val** approach
- Dataset for verification and validation of L2 products
- Definition of the **Production Model**
- Execution of **Cal/Val** plans for during E1 phase
- Foster the creation of a **ROSE-L L2 Ocean Open-Science community**
- **Harmonization** with **Sentinel-1** and **Harmony**

ROSS-Rachel objectives:

- Consolidation of L-band GMFs (HH, VV, VH) for nominal and extreme wind retrieval
- Wind field product performance verification
- Consolidation of L-band Modulation Transfer Function (MTF) for wave spectrum
- Swell performance assessment

Wind field retrieval scheme

- Bayesian approach in both nominal and extreme conditions
- Modular construction of a-posteriori Probability Distribution Function (PDF)

  $p\left(\vec{v}|\vec{v}_B, \psi_i\right) \propto p(\vec{v}_B) \prod_i p\left(\psi_i|\psi_i^S\right)$

  $\vec{v}_B$: Background wind term

  $p(\vec{v}_B)$: a-priori PDF of $\vec{v}_B$

  ψ_i: SAR-derived geophysical parameter:
  - $\sigma_0^{HH,HV,VV}$
  - Doppler Centroid Anomaly (DCA)
  - Relative wind direction (ϕ) (from Machine Learning)
  - Azimuth wavelength cut-off (λ_C)
  - Co-Cross Pol Correlation (CCPC) coefficient

  ψ_i^S: Simulated geophysical parameter

Cost Function minimizion

$$J(\vec{v}) = \left(\frac{\sigma_0 - \mathrm{CMOD}(\vec{v})}{\Delta\sigma_0}\right)^2 + \left(\frac{f^{DA} - \mathrm{CDOP}(\vec{v})}{\Delta f^{DA}}\right)^2 + \left(\frac{\lambda_C - \lambda_C^{20^o}}{\Delta\lambda_C}\right)^2$$

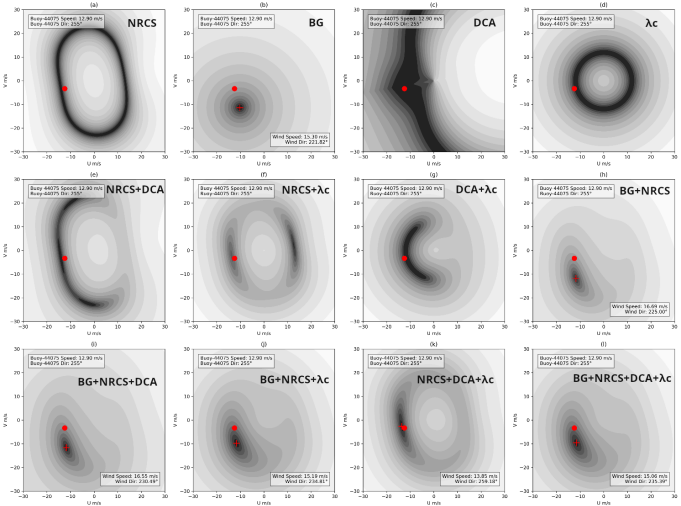

Contribution of individual cost function terms
Shading: Darker areas represent lower cost values

Markers:
- Red circle: Ground-truth wind vector from buoy
- Red cross: Retrieved wind vector

Subplots :
(a) NRCS
(b) Background wind model (BG)
(c) Doppler Centroid Anomaly (DCA)
(d) Azimuth cutoff (λ_C)
(e) NRCS + DCA
(f) NRCS + λ_C
(g) DCA + λ_C
(h) BG+NRCS
(i) BG+NRCS+DCA
(j) BG+NRCS+λ_C [1]
(k) NRCS+DCA+λ_C
(l) BG+NRCS+DCA+λ_C

[1] Y. Zhu et al. 2024, "On the Use of Azimuth Cutoff for Sea Surface Wind Speed Retrieval From SAR," in IEEE JSTARS, vol. 17, pp. 10367-10379, 2024, doi: 10.1109/JSTARS.2024.3407115.

Validation against scat (NRCS+DCA+λ_C)

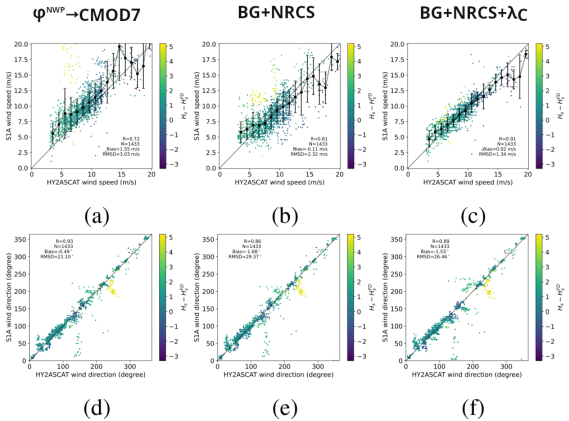

Fig. 7. Scatterplots of winds retrieved from the Sentinel-1 GRD data using (a) and (d) CMOD7, (b) and (e) optimal scheme, and (c) and (f) proposed scheme against the collocated HY2A-SCAT speeds (top) and wind directions (bottom). The colour is proportional to the difference between H_{s} and $H_{\mathrm{s}}^{\mathrm{FD}}$.

Validation against buoys (NRCS+DCA+AC)

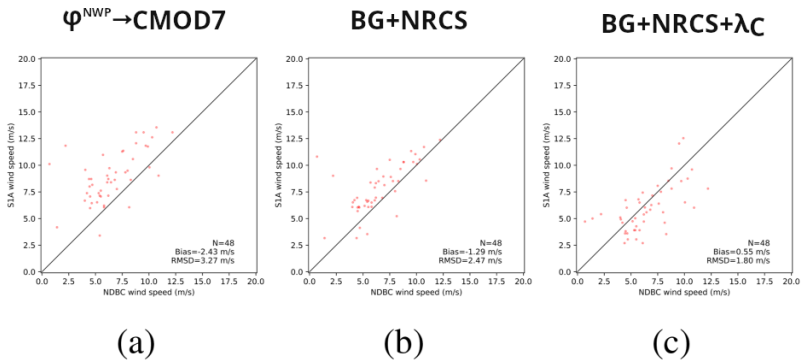

Fig. 8. Scatterplots of retrieved wind speeds from the Sentinel-1 GRD data using the (a) CMOD7, (b) optimal, and (c) proposed schemes against the collocated NDBC wind speeds.

Joint wind/current retrieval from S-1

$$J(\vec{v}, c_r) = \left(\frac{\sigma_0 - \mathrm{CMOD}(\vec{v})}{\Delta\sigma_0}\right)^2 + \left(\frac{f^{DA} - \mathrm{CDOP}(\vec{v}) - \frac{2sin\theta}{\lambda_e}}{\Delta f^{DA}}\right)^2 + \left(\frac{\vec{v} - \vec{v}_B}{\Delta\vec{v}}\right)^2 + \left(\frac{c_r - c_{r,B}}{\Delta c_r}\right)$$

$$J_{phys} = \left(\frac{c_r - c_r^{exp}(\vec{v})}{\sigma_{phys}}\right)^2$$

$$c_r^{exp} = \gamma|\vec{v}|cos(\alpha_c^{exp} - \alpha_{rad})$$

$$\alpha_c = \alpha_{to} + \mathrm{sgn}(f)\theta_E$$

$$\min_{\vec{v}, c_r}\{J + J_{phys}\}$$

c_r Ocean Surface Current (OSC)

c_r^{exp} Model surface current

α_c^{exp} Ekman-consistent current direction

α_{to} relative wind direction

f Coriolis parameter

θ_E Ekman deflection angle

[2] Zhu et al., "Integrated retrieval of ocean surface wind and current fields from single-look SAR observations through a physically constrained Bayesian framework", *under review* IEEE TGRS

Validation against HSCAT

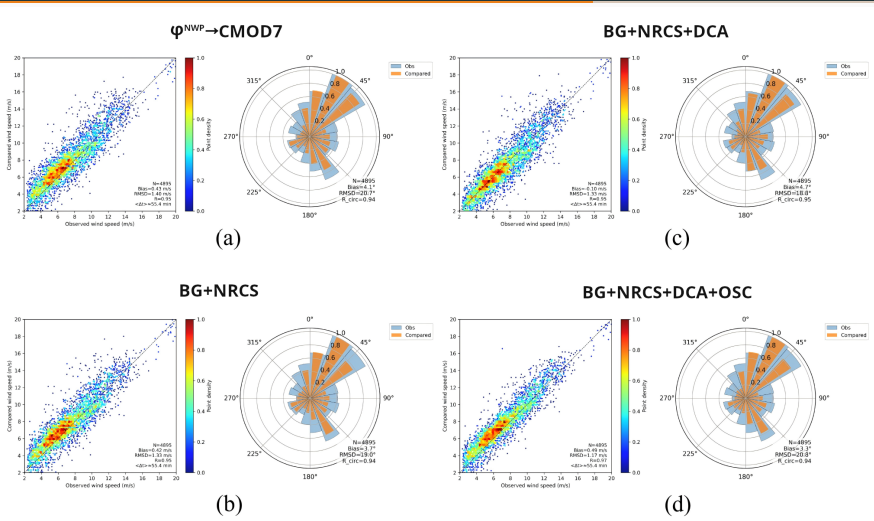

Figure 4: Comparison of wind fields with HYSCAT scatterometer observations. All collocations satisfy a temporal separation within 1 h, yielding 4 895 matched samples for each method.

Validation against buoys

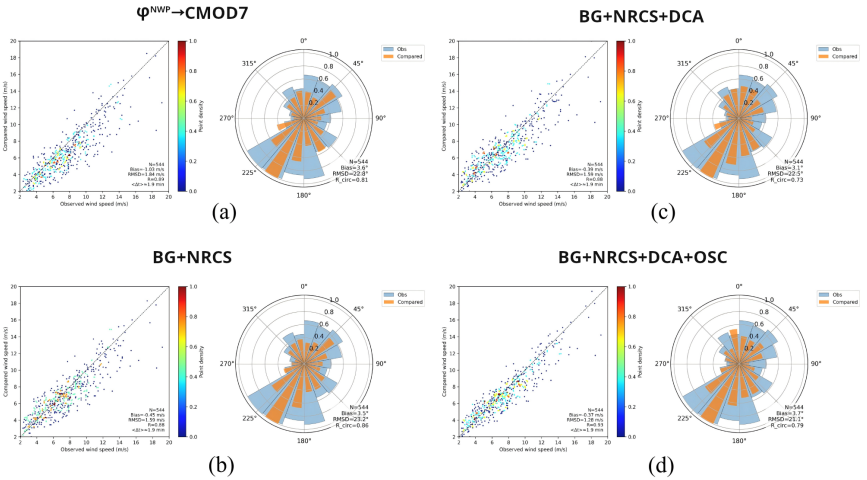

Figure 5: Comparison of wind fields with in situ wind measurements from NDBC buoys. SAR–buoy collocations are constrained within approximately 2 min, yielding 585 matched samples for each method.

Validation of radial OSC against HF radar

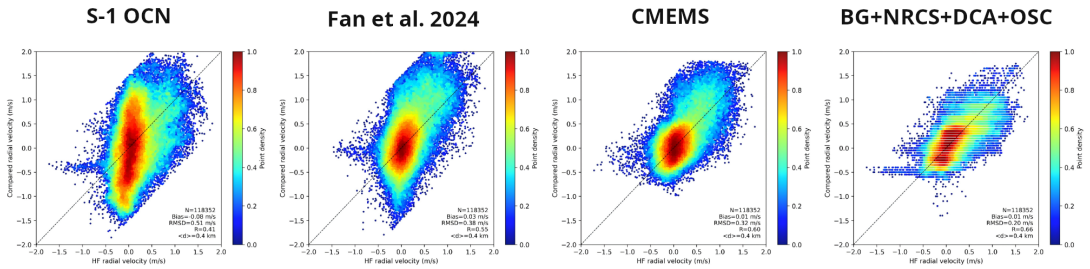

Figure 6: Comparison between SAR-derived radial surface currents and HF radar observations for four different approaches. Each panel shows a scatter plot of retrieved versus HF radar radial currents, with the one-to-one reference line indicated. The color scale represents the difference between retrieved and observed radial velocities.

S. Fan, B. Zhang, V. Kudryavtsev, and W. Perrie. Mapping radial ocean surface currents in the outer core of Hurricane Maria from synthetic aperture radar Doppler measurements. IEEE J. Sel. Top. Appl. Earth Obs. Remote Sens., 17:2090–2097, 2023.

Future plan

- Develop a ML scheme for wind direction retrieval
- Consolidate/Refine LMOD GMF for VV, HH and VH channels (ROSS)
- Fit L-band GMF for CCPC
- Fit L-band GMF for iMACS
- Investigate the possibility of a joint wind/surface current retrieval in the L-band

Back-up slides

Co-Cross Polarization Correlation Coefficient (CCPC)

$$\sigma_0^{VH} = aU + b$$

$$\rho_{VVVH} = \frac{< \sigma_0^{VV} \sigma_0^{VH*} >}{\sqrt{< |\sigma_0^{VV,2}| >< |\sigma_0^{VH,2}| >}}$$

- ρ_{VVVH} is the CCPC, also known as Polarization Correlation Coefficient (PCC) [3]
- * stands for Complex Conjugate
- U is the wind speed

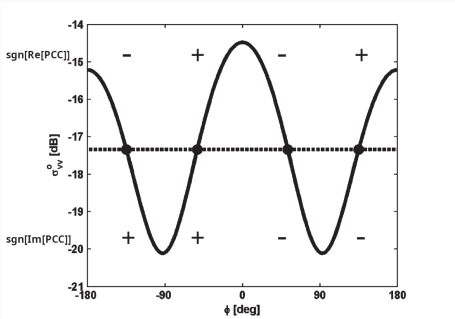

Fig. 1. (Black dots) All four relative wind direction solutions ϕ, $\pi - \phi$, $-\phi$, and $-(\pi - \phi)$ for the same NRCS in VV polarization (σ^o_{VV}) corresponding to an assumed wind speed of 10 m/s and an incidence angle of 45°, calculated by the CMOD5.N model. (Dashed line) Directional ambiguity of the model.

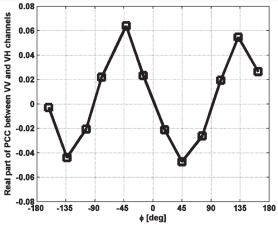

Fig. 5. RADARSAT-2 measured real part of the PCC between VV and VH channels versus relative wind direction. The average wind speed and incidence angle are 10 m/s and 35°, respectively.

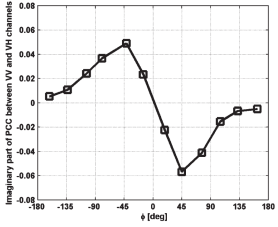

Fig. 6. RADARSAT-2 measured imaginary part of the PCC between VV and VH channels versus relative wind direction. The average wind speed and incidence angle are 10 m/s and 35°, respectively.

[3] B. Zhang et al., "Ocean Vector Winds Retrieval From C-Band Fully Polarimetric SAR Measurements," in IEEE Transactions on Geoscience and Remote Sensing, vol. 50, no. 11, pp. 4252-4261, Nov. 2012, doi: 10.1109/TGRS.2012.2194157

imaginary part of Mean Cross Spectrum (iMACS)

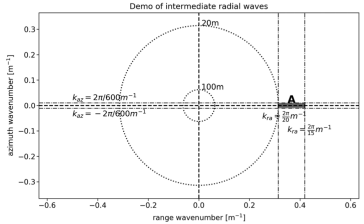

Figure 3. A schematic view of intermediate radial waves denoted by **A** over the mean cross-spectra is estimated. The limits of wavelength used in this study is 600 m in azimuth and between 15 and 20 m in range. The dotted circles represent wavelengths of 100 and 20 m from inner to outer.

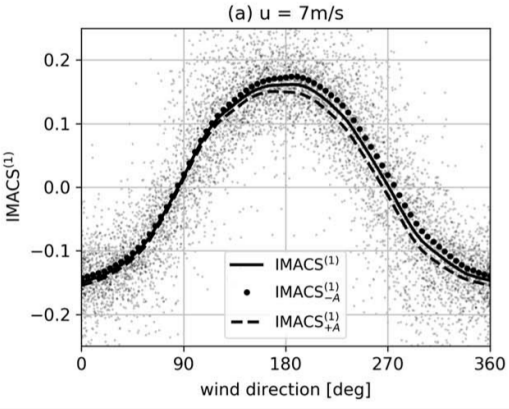

Some complementarity with CMOD

[4] Li, H., Chapron, B., Mouche, A. A., & Stopa, J. E. (2019). A new ocean SAR cross-spectral parameter: Definition and directional property using the global Sentinel-1 measurements. Journal of Geophysical Research: Oceans, 124, 1566–1577. https://doi.org/10.1029/2018JC014638